Theoretical Study on the Photochemical Behavior of Diphenylacetylene in the Low-Lying Excited States

Yoshiaki Amatatsu* and Masaru Hosokawa

Faculty of Engineering and Resource Science, Akita University, Tegata Gakuen-cho, Akita 010-8502, Japan

Received: June 21, 2004; In Final Form: August 27, 2004

Ab initio complete active space self-consistent field (CASSCF) and second-order multireference Möller−Plesset (MRMP2) calculations have been performed to examine the photochemical behavior of diphenylacetylene (DPA) theoretically. The stable structure of DPA in S_0 (S_0-geometry) is optimized to be D_{2h}. DPA at S_0-geometry is mainly excited into the $S_3(B_{1u})$ state and then relaxes into the stable geometry in the B_{1u} state (B_{1u}-geometry) which is characterized as a quinoid structure. The B_{1u}-geometry further relaxes into the globally stable geometry in S_1 (tS_1-geometry) which takes a trans-bent form. Around tS_1-geometry, DPA moves into the lowest triplet state through intersystem crossing and finally relaxes into the stable geometry in T_1 with D_{2h}. The vibrational analyses at the important conformations mentioned above are in good agreement with the experimental findings of time-resolved transient spectroscopy.

I. Introduction

The photochemical behaviors of aryl alkynes have been extensively studied by experiment and theory. In most cases, however, reasonable pictures have not been established yet. We recently examined the photochemical behavior of phenylacetylene (PA), as a prototype of aryl alkynes, by means of ab initio complete active space self-consistent field (CASSCF) and second-order Möller−Plesset perturbation (MRMP2) calculations.[1] In the present paper, we report the photochemical behavior of diphenylacetylene (DPA) as another prototype of aryl alkynes from the viewpoint of theoretical calculations. In the following paragraphs, we make a brief review of the previous studies on DPA.

The stable structure of DPA in S_0 is the starting point of the photochemistry. Many experimental data, such as X-ray diffraction[2] and infrared and Raman spectra,[3,4] gave evidence that DPA has D_{2h} symmetry in S_0. This experimental finding was also confirmed by means of ab initio calculations at the restricted Hartree−Fock level.[5] The electronic structures at the stable geometry were the main interest in the early stage of the research on the photochemistry of DPA. Tanizaki et al. measured the dichroic absorption spectrum so as to assign the absorption band to the B_{1u} state with the long axis polarized.[6] With the aid of excitation fluorescence and multiphoton ionization spectra, Okuyama and co-workers found that there are three excited states including the B_{1u} state within a few hundred cm^{-1}.[7] Gutmann et al. came to the same conclusion that three electronic states in the first excited manifold are close together.[8] The order of the electronic states in the condensed phase is, however, different from that in the supersonic jet. That is, the B_{1u} state is the first excited state in the condensed phase. Borst et al. recently reported the geometrical structure in the excited state as well as the ground state by means of the rotationally resolved fluorescence excitation spectrum.[9]

Picosecond time-resolved absorption spectroscopy gave more detailed information on the temporal behavior of electronically excited DPA. Hiura et al. measured the time-resolved Raman spectrum of the lowest triplet species with the lifetime of ∼1 μs.[3] The acetylenic CC stretch of the triplet species is observed at 1974 cm^{-1} which is abnormally lower than that of a normal acetylenic bond. Hirata et al. referred to a new fact that two intermediate species contribute to the photochemistry of DPA.[10,11] Upon electronic excitation into S_2, the short-lived species with the lifetime of 8 ps first forms and then changes into the long-lived species (200 ps) in S_1. The lifetime of the short-lived species is strongly dependent on the excitation energy as well as the temperature, while that of the long-lived one is independent. From the finding of the temperature dependence of the lifetime of the short-lived species, they estimated the energy barrier between the two species to be 890 cm^{-1}. It was also found that the triplet formation is observed after a raise time of 200 ps. In other words, the singlet long-lived species is a precursor of the triplet. Ferrante and co-workers examined Hirata's model by semiempirical calculations and fluorescence quantum yield measurements.[12] The electronic state of the short-lived species is assigned to B_{1u}. With the elongation of the central acetylenic bond, however, the B_{1u} state destabilizes and another state of A_u stabilizes so that the short-lived species of DPA changes into the long-lived species (A_u) with some barrier.

Contrary to the previous models that the photochemical reaction precedes under the D_{2h} geometry, Ishibashi et al. gave a new insight into the photochemistry of DPA by means of picosecond time-resolved transient coherent anti-Stokes Raman spectroscopy.[13−15] The long-lived species can take a trans-bent structure where the central CC bond turns to be an ethylenic double bond. On the other hand, the short-lived species keeps a linear acetylene-like geometry and the CC bond substantially has triple bond character, though the vibrational frequency (2099 cm^{-1}) is lower than that in S_0 (2220 cm^{-1}). With the decay of the singlet long-lived species, a new band assigned to the central CC stretches emerges at 1974 cm^{-1}. In agreement with the previous discussion on the triplet state,[3] they also supported that the triplet stable geometry is linear acetylene-like.[16]

Despite much information on various conformations of DPA, as mentioned above, the previous studies are not always

* To whom correspondence should be addressed. E-mail: amatatsu@ipc.akita-u.ac.jp. Fax: 81-18-889-2601.

10.1021/jp047308n CCC: $27.50
Published on Web 10/19/2004

reasonably united with each other for a picture of DPA photochemistry. So our present purpose is to propose a new and reasonable picture of the photochemical behavior of DPA in the low-lying excited states by means of reliable ab initio methods of CASSCF and MRMP2. The present paper is organized as follows. In the next section, we describe the computational strategy based on preliminary configuration interaction (CI) results. In section III, we mention the electronic structures at important conformations of DPA. Then we discuss how DPA travels from the Franck−Condon (FC) region into the globally stable geometry in S_1 and finally relaxes into the stable geometry in T_1. We also make comparison of the photochemistry of DPA with that of PA as well as other π-conjugated systems already studied by us. Last of all, we give a summary on the present computational results.

II. Method of Calculations

The CASSCF calculation which allows all possible excitations from the eight π-type occupied orbitals to the lowest eight unoccupied ones (i.e., (16,16)CASSCF) is desirable to do a quantitative discussion on the electronic structure and dynamics of electronically excited DPA. This calculation is, however, practically prohibited even on a high-performance computer, especially in the case of a global search of potential energy surfaces, geometry optimizations, and vibrational analyses. So how to reduce the computational labor is important in ab initio molecular orbital (MO) calculations of the excited states of DPA. Our strategy for the present calculations of DPA is similar to our previous calculations of polyenes or polyynes and their derivatives.[1,17−21] That is, in the first step, we did CI calculations at various geometries which cover the conformations possibly contributing to the photochemistry of DPA. In the present preliminary CI calculations, the following are found:

(i) The low-lying excited states for all the conformations sampled here are well described by the configuration state functions (CSFs) of the excitations among the highest five occupied π and the lowest five unoccupied π^* orbitals.

(ii) The nature of a set of these 10 π-type orbitals is invariant irrespective of the conformations.

Based on these CI results, we adopted CASSCF with 10 electrons in 10 orbitals (denoted by (10,10)CASSCF) for the scanning of the global potential energy surfaces. In necessity, we made energetic correction by means of the MRMP2 method. First, we optimized the geometry in S_0 by means of a state-specific (10,10)CASSCF. As discussed in detail later, the optimized geometry in S_0 (denoted by S_0-geometry) has D_{2h} symmetry. Then we optimized other important conformations, such as the stable geometry for each excited state in the FC region, the conical intersection, and the globally stable geometries in S_1 and T_1. To examine the dynamical behavior, we followed the reaction path from the FC region into the globally stable geometry in S_1. At several important conformations, we did vibrational analyses so as to directly compare the calculated results with the experimental data.

We used the GAMESS program in the present ab initio calculations,[22] except for the location of the conical intersection by Gaussian 03.[23] The basis set used in the calculations is the Huzinage−Dunning double-ζ basis set augmented by polarization ($\alpha_d = 0.75$) on carbon atoms.

III. Results and Discussion

We begin by mentioning the electronic structures of DPA at S_0-geometry under D_{2h} symmetry. In Table 1, we list the electronic structures in the low-lying excited states. To understand the character of the electronic structure and the symmetry for each state, we show the relevant MOs in Figure 1. The $S_1(B_{2u})$ and $S_2(B_{3g})$ states can be assigned to the local $\pi-\pi^*$ excitations within each benzene ring. The S_3 state (B_{1u}), which is well described by the HOMO−LUMO single excitation (HOMO, highest occupied MO; LUMO, lowest unoccupied MO), can be characterized as the $\pi-\pi^*$ excitations originating from the central acetylenic triple bond, of which both π and π^* orbitals are out of the DPA plane. The S_4 state with A_u also

TABLE 1: Excitation Energies, Oscillator Strengths, and the Main CSFs of DPA at S_0-Geometry

	excitation energy (in eV)[a]	oscillator strength[b]	main CSFs[c]
$S_0(A_g)$[d]	0.0 (0.0)		0.923(closed shell)
$S_1(B_{2u})$	6.056 (4.054)	1×10^{-6}	0.520(1−2′) −0.508(2−1′) −0.320(4−3′)−0.302(3−4′)
$S_2(B_{3g})$	6.061 (4.052)	0.0	0.507(3−1′)+0.517(1−3′) −0.323(4−2′)+0.302(2−4′)
$S_3(B_{1u})$	6.407 (4.507)	0.873	0.925(1−1′)
$S_4(A_u)$	6.688 (4.847)	0.0	0.940(5−1′)

[a] The values in the parentheses are obtained by MRMP2 corrections. [b] The values are given in the velocity form. [c] The CSFs of which absolute values of CI coefficients are greater than 0.3 are listed. Five occupied π orbitals and the lowest four unoccupied π^* ones in the order of energy are designated by 5,4,3,2,1(HOMO),1′(LUMO),2′,3′,4′, 5′, respectively. 1−1′ in parentheses, for instance, indicates the CSF of single excitation from orbital 1 to 1′. [d] The symmetry label of each electronic state is under D_{2h}.

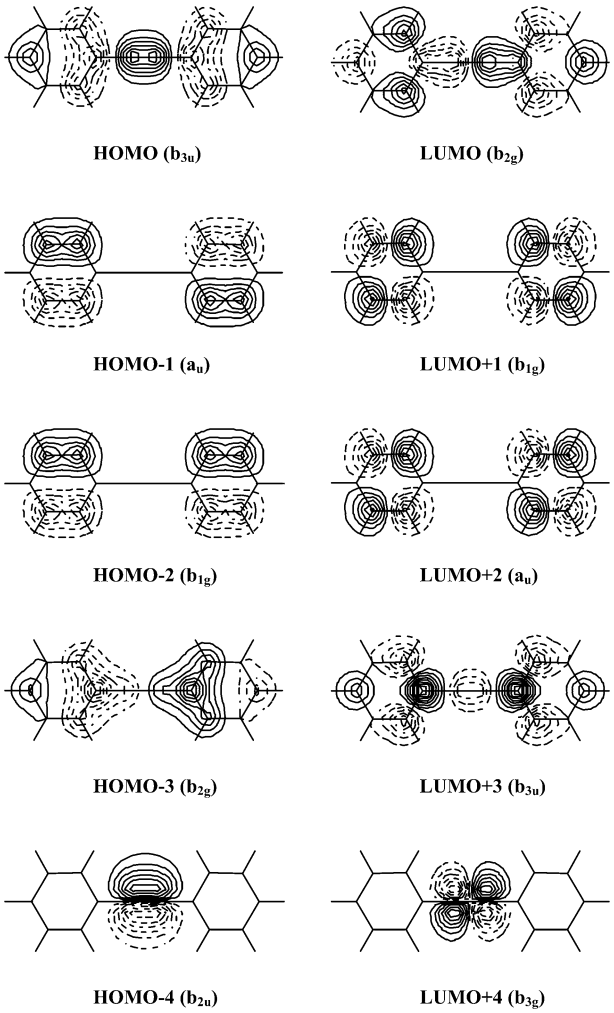

Figure 1. Molecular orbitals and their symmetry labels (under D_{2h}) relevant to the low-lying excited states at S_0-geometry.

TABLE 2: Characteristic Optimized Parameters of DPA

geometry	S_0	B_{2u}	B_{3g}	B_{1u}	A_u	tS_1	S_2/ S_1-CIX	T_1
				Bond Distances (in Å)				
$R(C^{\alpha}-C^{\alpha'})$	1.204	1.217	1.217	1.260	1.290	1.357	1.298	1.251
$R(C^{1}-C^{\alpha})$	1.449	1.409	1.410	1.380	1.382	1.425	1.394	1.363
$R(C^{1}-C^{2})$	1.402	1.439	1.439	1.432	1.427	1.422	1.423	1.454
$R(C^{2}-C^{3})$	1.395	1.423	1.423	1.382	1.388	1.389	1.381	1.380
$R(C^{3}-C^{4})$	1.390	1.388	1.388	1.401	1.393	1.404	1.396	1.402
$R(C^{4}-C^{5})$	1.390	1.388	1.388	1.401	1.393	1.392	1.398	1.402
$R(C^{5}-C^{6})$	1.395	1.423	1.423	1.382	1.388	1.384	1.379	1.380
				Bond Angles (in Degrees)				
$\alpha(<C^{1}C^{\alpha}C^{\alpha'})$	180.0	180.0	180.0	180.0	180.0	127.9	157.5	180.0

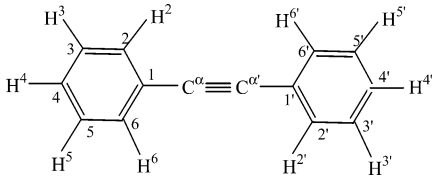

Figure 2. Numbering of atoms in DPA.

has similar character with the $\pi-\pi^*$ excitation relevant to the central acetylenic bond, although the π orbital is in the DPA plane. The excitation energies and oscillator strengths can be discussed in close relation to the experimental absorption spectrum. At the CASSCF level, the excitation energies of the low-lying excited states are close to each other but they are too high for the first broad absorption band in the range of 250−300 nm (i.e., 4.13−4.96 eV).[10,12] However, after MRMP2 energetic corrections, they settle down the energy range of the absorption band. As to the transition intensity, contrary to the previous discussion that the main transition is S_0-S_2,[10,11,14,15] the main transition among the low-lying excited states is S_0-S_3, which is long-axis (i.e., *a*-axis) polarized. Another transition of S_0-S_1 is very weak, and the others of S_0-S_2 and S_0-S_4 are forbidden.

Next we mention the stable geometries in the FC region. In Table 2, we list the optimized parameters for each state under D_{2h} symmetry as well as those at other important conformations. The numberings of atoms are shown in Figure 2. The bond distance of $R(C^{\alpha}\equiv C^{\alpha'})$ (1.204 Å) at S_0-geometry with A_g is calculated to be very similar to that of a normal C≡C triple bond. On the other hand, the linkage bond of C^1-C^{α} (1.449 Å) is slightly shorter than a normal C−C single bond, which is due to some resonance between the phenyl group and the triple bond of $C^{\alpha}\equiv C^{\alpha'}$. Furthermore, the CC bond distances of the phenyl groups (ca. 1.40 Å) take intermediate values between normal single and double bond distances, which are close to that of aromatic benzene. These features are found in the relevant parts of PA.[1] The B_{2u}-geometry, which is obtained by the optimization of DPA with B_{2u} under constraint of D_{2h}, is characterized as the enlargement of the benzene rings. That is, the CC bond distances in the benzene rings are longer than those at S_0-geometry. This is due to the local $\pi-\pi^*$ excitation within each benzene ring. In other words, the occupied π electrons in the benzene ring are excited into unoccupied π^* orbitals, which leads to a weakening and elongation of the relevant CC bonds in the benzene ring. This feature is also found in those of PA and styrene.[1,18] The optimized geometry with B_{3g} also has similar character to that of B_{2u}. The interpretation is the same as that for B_{2u}. The optimized geometry with B_{1u} (B_{1u}-geometry) has the following features: (i) the benzene rings are characterized as a quinoid structure where the aromaticity of the benzene ring is lost, and (ii) the central acetylenic bond (1.260 Å) is much longer, while the linkage bonds (1.380 Å) are much shorter. These features are understandable in relation to the electronic structure of B_{1u}. As mentioned above, the B_{1u} state is well described by the HOMO−LUMO single excitation (refer to Figure 1). So the out-of-plane π-orbitals in the central acetylenic bond change from bonding into antibonding character upon electronic excitation so that the $C^{\alpha}C^{\alpha'}$ elongates. On the other hand, the out-of-plane π-type orbitals in the linkage bonds of C^1C^{α} and $C^{1'}C^{\alpha'}$ change from antibonding into bonding character so that the linkage bonds shrink. This explanation about B_{1u}-geometry, in a sense, is the same as that of the stable geometry of PA in S_2 under constraint of C_{2v}.[1] The stable geometry with A_u (A_u-geometry) is similar to that with B_{1u}. This is natural because both the B_{1u} and A_u states are originated by the excitations from the central acetylenic π orbitals and the only difference between them is that the electron is excited from an out-of-plane (for B_{1u}) or an in-plane (for A_u) occupied π orbital. To check the validity of the stable geometries, we compared the calculated rotational constants with experimental ones. In Table 3, we list the calculated rotational constants at each geometry as well as the experimental ones.[9] The calculated rotational constants at S_0-geometry well reproduce the experimental ones in S_0. According to the dispersed fluorescence excitation spectrum, the rotational constants at B_{1u}-geometry are also in good agreement with the experimental ones. However, those at other geometries in the excited states are similar to them. So we can conclude that the rotational constants are not always deterministic to validate the stable B_{1u}-geometry in the excited state at our present level of calculations.

TABLE 3: Rotational Constants (in MHz) of DPA at Each Geometry

geometry	constant	calculation	experiment[a]
S_0	*A*	2860.1	2861.7
	B	246.9	249.0
	C	227.3	229.0
B_{1u}	*A*	2797.9	2820.6
	B	250.2	251.3
	C	229.6	228.6
B_{2u}	*A*	2799.2	
	B	245.7	
	C	225.8	
B_{3g}	*A*	2799.5	
	B	245.5	
	C	225.7	
A_u	*A*	2826.8	
	B	247.5	
	C	227.6	

[a] The values were taken from ref 9.

The globally stable structure in S_1 is found to take a trans-bent form with A_u under C_{2h} symmetry (tS_1-geometry), as seen in Table 2 ($\angle C^1C^{1'}C^{\alpha'} = 127.9°$, not 180.0°). This is in agreement with an experimental finding that the globally stable structure in S_1 has C_i or C_{2h} symmetry because of the mutual exclusion rule between infrared and Raman spectra.[15] The characteristic geometrical parameters are as follows. The $C^{\alpha}C^{\alpha'}$ bond (1.358 Å) elongates up to a normal double bond. The linkage bond distances of C^1C^{α} and $C^{1'}C^{\alpha'}$ (1.425 Å) are longer than those at B_{1u}-geometry. Therefore, tS_1-geometry is like *trans*-stilbene. In Table 4, we list the electronic structures at tS_1-geometry. The S_1 state is well described by the HOMO−LUMO single excitation. As shown in Figure 3, the HOMO with a_u is, roughly speaking, a π orbital concerning the central ethylenic double bond. The LUMO with a_g is relevant to the unpaired electrons originating from the in-plane orbitals. So we conclude that S_1 at tS_1-geometry has diradical character.

Now we discuss how DPA changes into the globally stable tS_1-geometry in S_1 after the main transition into $S_3(B_{1u})$. In this

TABLE 4: Relative Energies and the Main CSFs at tS$_1$-Geometry

	relative energy (in eV)[a]	main CSFs[b]
S_0	1.682 (1.158)	0.882(closed shell)−0.303(5^2-$1'^2$)
S_1	5.094 (3.098)	0.944(1−1′)
T_1	4.226 (2.635)	0.923(1−1′)

[a] The energies are relative to that in S_0 at S_0-geometry. The values are obtained by means of (10,10)CASSCF and MRMP2 (in parentheses). [b] The CSFs of which absolute values of CI coefficients are greater than 0.3 are listed. Five occupied π orbitals and the lowest four unoccupied π^* orbitals in the order of energy are designated by 5,4,3,2,1(HOMO),1′(LUMO),2′,3′,4′,5′, respectively. 1−1′ in parentheses, for instance, indicates the CSF of single excitation from orbital 1 to 1′.

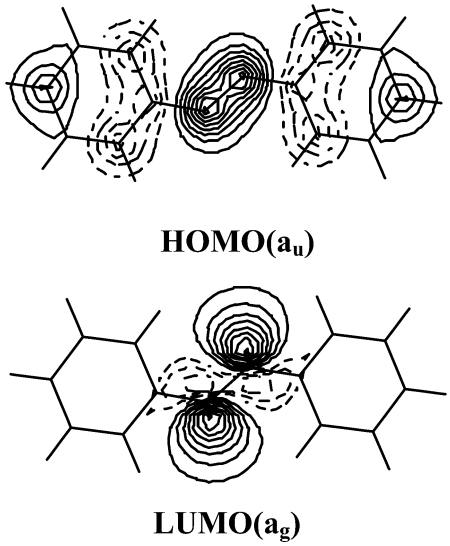

Figure 3. HOMO, LUMO, and their symmetry labels (under C_{2h}) at tS$_1$-geometry.

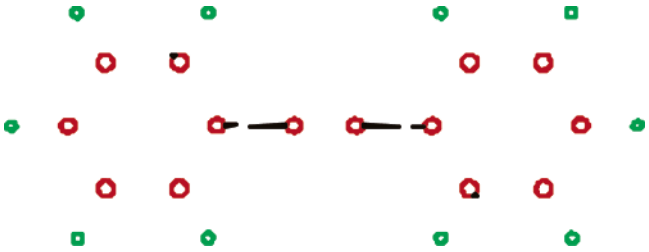

Figure 4. Force acting on each atom in $S_3(B_{1u})$ at S_0-geometry.

paragraph, we focus on the photochemical behavior in the FC region. In Figure 4, we show the force acting on each atom after electronic excitation into $S_3(B_{1u})$ at S_0-geometry. From this figure, the geometrical change of DPA upon electronic excitation is expected to be elongation of the central $C^{\alpha}C^{\alpha'}$ bond as well as the shrinkage of the linkage bonds of C^1C^{α} (and $C^{1'}C^{\alpha'}$). This implies that DPA in B_{1u} at S_0-geometry tends to change into the B_{1u}-geometry mentioned above. In Table 5, we list the relative energies at each stable geometry in the FC region. For CASSCF calculations, the S_1 states at the B_{2u}-, B_{3g}-, and B_{1u}-geometries are energetically lower than the $S_3(B_{1u})$ state where DPA at S_0-geometry is mainly excited into. However, if we consider the above discussion on the force acting on DPA in $S_3(B_{1u})$ at S_0-geometry, DPA is likely to relax into B_{1u}-geometry in S_1 in the FC region. Incidentally, we also listed the energies by means of MRMP2 in Table 5. The energies are shifted down, but it is found that the energy corrections (i.e., E(MRMP2) − E(CASSCF)) for each electronic state and geometry are almost constant (ca. 2 eV). In other words, the discussion based on more sophisticated MRMP2 calculations is expected to be similar to that of CASSCF results, though the potential energies by MRMP2 are only realistic in comparison with the experimental energies.

The next concern is how the B_{1u}-geometry in the FC region changes into the globally stable tS$_1$-geometry. In Figure 5, we present the three possible reaction paths schematically. Path I is an "in-plane" mechanism where DPA changes from B_{1u}- into tS$_1$-geometry keeping planar structure. In Figure 6, we show the potential energy curves with respect to the bending angle of $\angle C^1C^{\alpha}C^{\alpha'}$, where other parameters are optimized under constraint of C_{2h}. Here we should make a comment on the change of the symmetry from D_{2h} into C_{2h}. Under D_{2h} symmetry, the principal axis is parallel to the triple bond of $C^{\alpha}C^{\alpha'}$, while it is perpendicular to the DPA plane under C_{2h}. So the B_{1u} state at B_{1u}-geometry is labeled as B_u under C_{2h} symmetry, while the A_u state is labeled as A_u even under C_{2h}. It can be seen that the B_u potential energy becomes unstable with the decrease of the bending angle $\angle C^1C^{\alpha}C^{\alpha'}$ and does not connect with the global minimum of tS$_1$-geometry with A_u. So we traced back from tS$_1$-geometry with A_u so as to find a conically crossing region around the bending angle of $180° - \angle C^1C^{\alpha}C^{\alpha'} \sim 25°$. Before further discussion based on the CASSCF results, it is worthwhile emphasizing again that the present CASSCF results are reliable enough to make a story of the photochemistry of DPA. In Figure 6b, we show the potential energy curves by means of MRMP2. It can be seen that the shapes of the potential energy curves are similar to those by the CASSCF method, though the energies are lower. This implies that, as pointed out in the last paragraph, a story of the DPA photochemistry by the costly MRMP2 method is not so different from that by CASSCF, except that the MRMP2 energies are realistic in comparison with experimental ones.

Now we are back to the main interest of the DPA photochemistry. Based on the result mentioned above, we searched for a conically crossing point between two surfaces (i.e., S_2/S_1-CIX) under C_1 symmetry. Here we tried to reduce computational labor by further selection of active orbitals because we have experience that the location of a conical intersection takes much more time than the location of a stable geometry or saddle point. In the crossing region, only the four orbitals (refer to Figure 7) are enough to describe the two states of interest. Therefore, we adopted the (4,4)CASSCF method for the location of S_2/S_1-CIX. To check the validity of the reduction of the active space, we listed the electronic structures by means of (10,10)CASSCF and MRMP2 at S_2/S_1-CIX. It is found that at most four active orbitals mentioned above well describe these electronic states and the energy difference is small enough to be a CIX (see Table 6). This implies that an S_2/S_1-CIX by means of much more costly calculation of (10,10)CASSCF or MRMP2 is similar to the present one. The S_2/S_1-CIX is optimized to be C_{2h} symmetry substantially, though we did not consider any symmetry restriction in the optimization step. From Table 2, it can be seen that the characteristic optimized parameters at S_2/S_1-CIX take intermediate values between B_{1u}- and tS$_1$-geometries. We also searched conically crossing points in paths II and III of Figure 5. Path II is an "out-of-plane" mechanism where the two phenyl rings first move out of the original DPA plane and then DPA reaches the stable tS$_1$-geometry through phenyl torsional motions as well as further bendings. Path III is the "rotation" mechanism where the two phenyl rings first rotate keeping the linear geometry and then DPA reaches the tS$_1$-geometry through bending as well as phenyl torsional motions. However, both of the optimized S_2/S_1-CIXs in paths

TABLE 5: Electronic States and Relative Energies in the FC Region under D_{2h} Symmetry

	geometry				
electronic state	S_0	B_{2u}	B_{3g}	B_{1u}	A_u
S_0	A_g(0.0,0.0)[a]	A_g(0.258,0.028)	A_g(0.256,0.028)	A_g(0.437,0.046)	A_g(0.581,0.105)
S_1	B_{2u}(6.056,4.054)	B_{2u}(5.820,3.792)	B_{2u}(5.820,3.793)	B_{1u}(5.961,3.927)	B_{1u}(6.010,3.935)
S_2	B_{3g}(6.061,4.052)	B_{3g}(5.827,3.790)	B_{3g}(5.827,3.791)	B_{2u}(6.081,3.867)	A_u(6.147,4.272)
S_3	B_{1u}(6.407,4.507)	B_{1u}(6.264,4.217)	B_{1u}(6.269,4.220)	B_{3g}(6.090,3.865)	B_{2u}(6.171,3.898)
S_4	A_u(6.688,4.847)	A_u(6.552,4.624)	A_u(6.557,4.627)	A_u(6.200,4.339)	B_{3g}(6.180,3.896)

[a] The first and second values in the parentheses are those by means of (10,10)CASSCF and MRMP2, respectively.

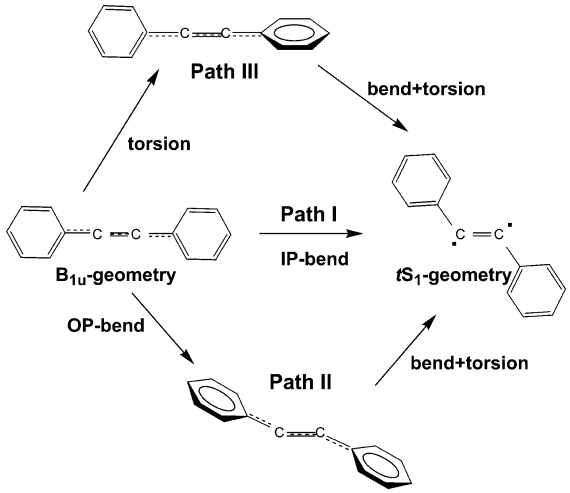

Figure 5. Possible reaction pathways from B_{1u}- into $t$$S_1$-geometry.

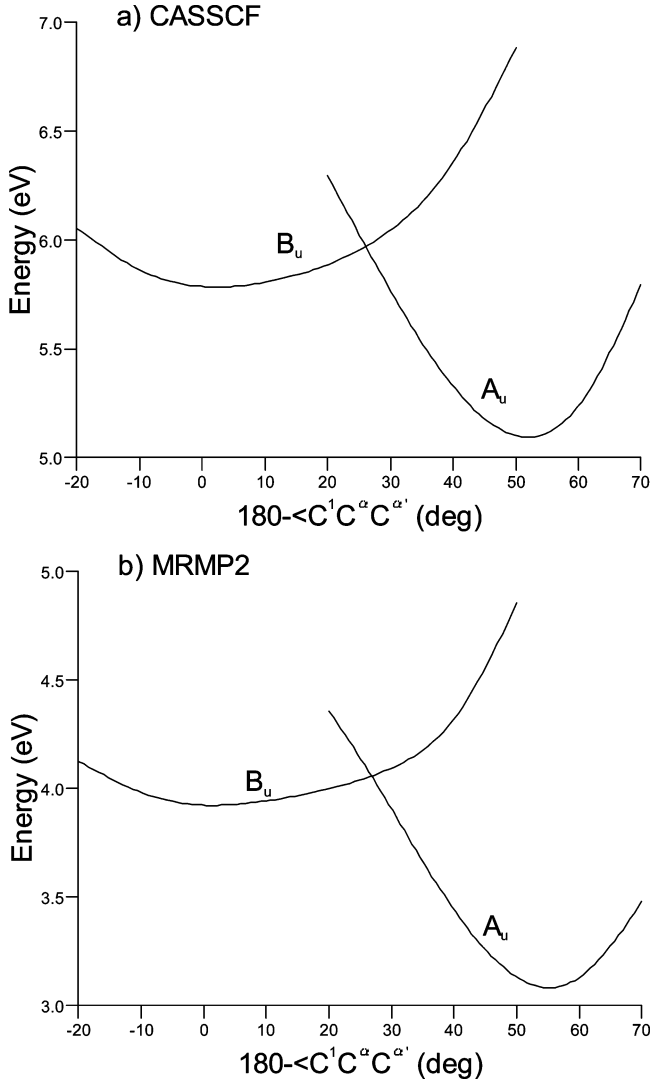

Figure 6. Potential energy curves with respect to the bending angle of $\angle C^1C^\alpha C^{\alpha'}$ by (a) CASSCF and (b) MRMP2. The other parameters are optimized under C_{2h} symmetry, and so the B_{1u} state at the linear geometry (i.e., $180° - \angle C^1C^\alpha C^{\alpha'} = 0°$) corresponds to the B_u state. The negative value in the abscissa means that DPA takes the cis-form under C_2 symmetry so that the B_u state corresponds to the B state.

II and III converged to substantially the same geometry in path I. This means that DPA must pass through S_2/S_1-CIX mentioned above, irrespective of paths I−III.

To know which of paths I−III is the most realistic, we followed the intrinsic reaction coordinate which S_2/S_1-CIX uniquely connects with both the starting point of B_{1u}-geometry and the final point of $t$$S_1$-geometry. It is found that DPA substantially keeps planar structure in the forward and backward reaction coordinates from S_2/S_1-CIX. Therefore, we conclude that path I is the most realistic. In Figure 8a, we show the energy profile along the reaction coordinate. It can be seen that there is a small energy barrier of 0.166 eV (relative to S_1 at B_{1u}-geometry). The MRMP2 value is 0.115 eV. This is not so different from an experimental estimation, 0.110 eV (890 cm^{-1}).[10] In Figure 8b, we show the characteristic geometrical parameters along the reaction coordinate. The bending angle $\angle C^1C^\alpha C^{\alpha'}$ proportionally changes along the reaction coordinate. In other words, it is proper to regard the bending angle as a reaction coordinate. As to the bond distances, the central $C^\alpha C^{\alpha'}$ and the linkage C^1C^α (and $C^{1'}C^{\alpha'}$) bonds drastically change in the vicinity of S_2/S_1-CIX. The $C^\alpha C^{\alpha'}$ quickly changes from a triple into a double bond. The linkage bonds elongate in accord with the elongation of $C^\alpha C^{\alpha'}$. On the other hand, the bond distances in the benzene rings are not so changed throughout the process from B_{1u}-geometry into $t$$S_1$-geometry (refer to the relevant part in Table 2). From these findings, we can point out a role of S_2/S_1-CIX in the dynamical behavior. One is that, at S_2/S_1-CIX, the B_{1u}-geometry with a triple bond character in the central $C^\alpha C^{\alpha'}$ bond is well separated from the globally stable $t$$S_1$-geometry with a double bond character. From the viewpoint of electronic structure, S_2/S_1-CIX serves to switch the electronic state of B_u into A_u. To see the dynamical process in comparison with transient infrared vibrational spectroscopic experiments,[14] we list the key vibrational frequencies of the $C^\alpha C^{\alpha'}$ stretches at important geometries and electronic states in Table 7. In S_0 at S_0-geometry, the vibrational frequency is calculated to be 2220 cm^{-1}, which is observed in the typical acetylenic bond region. At the intermediate B_{1u}-geometry, the vibrational frequency of the $C^\alpha C^{\alpha'}$ stretch is calculated to be 2100 cm^{-1} which is shifted down by ∼100 cm^{-1} from that in S_0. This is in good agreement with the experimental finding that the CC stretch of the transient species with 8 ps lifetime is observed at 2099 cm^{-1}. Once DPA overcomes the S_2/S_1-CIX, it quickly relaxes into the globally stable $t$$S_1$-geometry with a much longer lifetime (200 ps in experiment). The $C^\alpha C^{\alpha'}$ stretch of $t$$S_1$-geometry is calculated to be 1573 and 1554 cm^{-1}, which are in the typical ethylenic bond stretching region. Furthermore, we examined the isotope

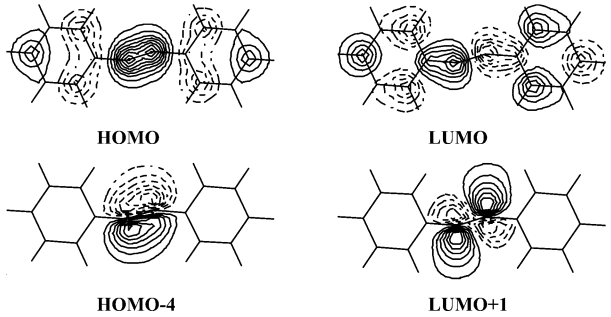

Figure 7. MOs relevant to the electronic structures at S_2/S_1-CIX. The MOs are obtained by (10,10)CASSCF at S_2/S_1-CIX. The lowest MO in the figure corresponds to HOMO-4, not HOMO-1 in (10,10)-CASSCF.

TABLE 6: Relative Energies and the Main CSFs at S_2/S_1-CIX

	relative energy (in eV)[a]	main CSFs[b]
S_1	6.127 (4.042)	0.916(1−1′)
S_2	6.311 (4.376)	0.952(1−2′)

[a] The energies are relative to that in S_0 at S_0-geometry. The values are obtained by means of (10,10)CASSCF and MRMP2 (in parentheses). [b] The CSFs of which absolute values of CI coefficients are greater than 0.3 are listed. Five occupied π orbitals and the lowest four unoccupied π^* orbitals in the order of energy are designated by 5,4,3,2,1(HOMO),1′(LUMO),2′,3′,4′,5′, respectively. 1−1′ in parentheses, for instance, indicates the CSF of single excitation from orbital 1 to 1′.

effects where the central two acetylenic normal carbons ^{12}C are replaced by ^{13}C. We obtained the vibrational frequencies by means of **GF** matrix diagonalizations where the force constant **F**-matrix is same as that of the normal species and the **G**-matrix is changed. The isotope effects of the key bands also reproduce the experimental ones.

As mentioned in the Introduction, the lowest triplet species forms with the decay of the long-lived species in S_1 at $t$$S_1$-geometry.[14,16] As listed in Table 4, the energy in T_1 at $t$$S_1$-geometry is not so different from that in S_1. This implies that DPA in S_1 is relaxed into T_1 through intersystem crossing in the vicinity of $t$$S_1$-geometry, though we did not optimize the crossing point actually. Once DPA changes from S_1 into T_1 around $t$$S_1$-geometry, DPA geometrically relaxes in T_1 with a much longer lifetime of $\sim$1 μs.[3,10,12,14,16] In Table 2, the optimized geometries in T_1 (T_1-geometry) with D_{2h} symmetry are also listed. The values are similar to those at B_{1u}-geometry as well as the previous computational result of restricted open-shell Hartree−Fock calculation.[5] The T_1 state at T_1-geometry (3.830 eV by CASSCF, 1.924 eV by MRMP2) is more stable than that at $t$$S_1$-geometry (refer to Table 4). The vibrational frequency of the $C^{\alpha}C^{\alpha'}$ stretch is in good agreement with the experimental one (see Table 7).[3,14]

Based on the above discussion, we propose a picture of the photochemistry of DPA, which is schematically shown in Figure 9. DPA with D_{2h} symmetry is mainly excited into $S_3(B_{1u})$ and relaxes into the linear B_{1u}-geometry characterized by a quinoid structure where the aromaticities of the benzene rings are lost. Since the B_{1u}-geometry is separated from the globally stable $t$$S_1$-geometry by a small energy barrier, DPA at B_{1u}-geometry has a short lifetime (8 ps in experiment) as an intermediate. Once DPA overcomes the barrier, DPA easily reaches $t$$S_1$-geometry which takes a trans-bent structure and has double bond character in the central CC bond. The $t$$S_1$-geometry with diradical character in S_1 has a much longer lifetime (200 ps in experiment). DPA further relaxes from S_1 into T_1 through intersystem crossing and then becomes stable at the D_{2h} linear geometry in T_1 ($\sim$1 μs in experiment).

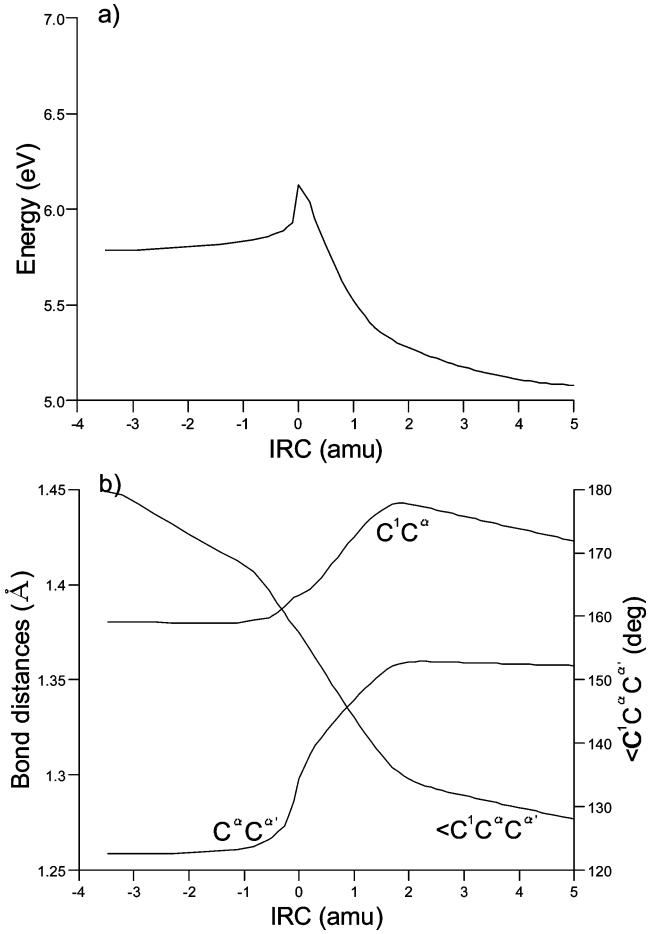

Figure 8. (a) Energy profile and (b) the characteristic geometrical parameters along the reaction coordinate, which is obtained by (10,10)CASSCF.

TABLE 7: Vibrational Frequencies (in cm^{-1}) of the $C^{\alpha}C^{\alpha'}$ Stretch Band[a]

electronic state	geometry	frequencies ^{12}C-species	frequencies ^{13}C-species[b]
S_0	S_0	2220(2220)[c]	2136
S_1	B_{1u}	2100(2099)	2067(2060)
S_1	$t$$S_1$	1573,1554(1577,1557)	1566,1540(1574,1535)
T_1	T_1	1980(1974)	1907(1942)

[a] The force constants are scaled down by 0.82 (S_0-geometry), 0.82 (B_{1u}-geometry), 0.87 ($t$$S_1$-geometry), and 0.88 ($T_1$-geometry), respectively. [b] Only C^{α} and $C^{\alpha'}$ carbons are substituted into the isotope ^{13}C. [c] The values in the parentheses are experimental ones taken from ref 14.

From the viewpoint of the photochemistry of acetylenoids, it is interesting to compare DPA with PA.[1] The main transition in the low-lying excited states is long-axis (i.e., parallel to the triple bond) polarized. The excited state with large transition intensity (S_2 for PA, S_3 for DPA) is well described by the HOMO−LUMO single excitation. In the excited state, the aromaticity of the benzene ring(s) is destroyed. However, these relaxation processes are different from each other. In the case of PA, the S_2/S_1-CIX is characterized by an allenoid structure where the β-H atom bonded to the acetylenic part comes to be located out of the remaining part. In other words, the out-of-plane motion of β-H is essential in the internal conversion from S_2 into S_1. On the other hand, electronically excited DPA first relaxes into the acetylenic linear B_{1u}-geometry and then changes

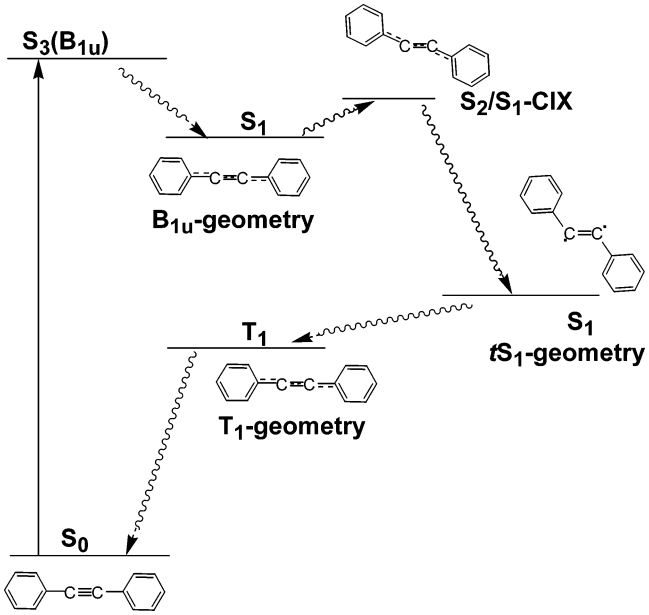

Figure 9. Schematic representation of the photochemistry of DPA.

into tS_1-geometry substantially keeping the planar C_{2h} structure. As to the absorption spectra, we can find out the similarity between PA and DPA. Both of them are characterized as a broad band with a few prominent peaks. In our previous study on PA,[1] we proposed that the peculiar peaks with constant intervals are due to the vibrational structure assigned to the stretching mode of the allenoid C═C═C structure which forms upon electronic excitation. In the case of DPA, the progression with the interval of 2150 cm^{-1} is tentatively assigned to the C≡C stretch by Hirata et al.[10] About this interpretation, we would like to make additional comment. As discussed in terms of HOMO and LUMO at S_0-geometry in the previous paragraph, the central $C^{\alpha}C^{\alpha'}$ triple bond weakens due to the electronic excitation into $S_3(B_{1u})$ and, therefore, the progression intervals of 2150 cm^{-1} are smaller than the vibrational frequency due to a normal C≡C stretch in S_0. Furthermore, the progression intervals are larger than the $C^{\alpha}C^{\alpha'}$ stretches of the intermediate short-lived species (2099 cm^{-1}). This implies that the central $C^{\alpha}C^{\alpha'}$ bond further weakens in the relaxation from S_0-geometry into B_{1u}-geometry within a few picoseconds upon electronic excitation.

Finally, we give our perspective of the common feature of the π-conjugated systems polyene and polyynes in the radiationless relaxation of photoisomerization or internal conversion. Up to now, we have examined the photochemistry of typical π-conjugated systems.[1,17−21] Thereby, it is found that the bond alternation of π-conjugated systems is essential for the radiationless relaxation of S_1-S_0 or S_n-S_1 ($n \geq 2$). We will further continue to check if the feature is commonly found in another π-conjugated system by means of ab initio methods.

IV. Concluding Remarks

In this paper, we reported the photochemical behavior of DPA in the low-lying excited states by means of ab initio CASSCF and MRMP2 calculations. The stable geometry in S_0 has D_{2h} symmetry. Upon electronic excitation into S_3 with B_{1u}, DPA tends to relax into an intermediate species with D_{2h} symmetry, which is characterized by a quinoid structure where the aromaticities of the benzene rings are lost and the central triple CC bond is slightly weakened. The globally stable DPA in S_1 takes a trans-bent form with double bond character in the central CC bond and has diradical character. In the vicinity of the stable trans-bent conformation, DPA in S_1 further relaxes into T_1 through intersystem crossing so that DPA with D_{2h} finally forms in T_1.

Acknowledgment. The numerical calculations were partly performed in the Computer Center of the Institute for Molecular Science. This work is financially supported by a Grant-in-Aid for Scientific Research (C) (No. 15550003) from the Ministry of Education, Culture, Sports, Science and Technology.

References and Notes

(1) Amatatsu, Y.; Hasebe, Y. *J. Phys. Chem. A* **2003**, *107*, 11169−11173.
(2) Espiritu, A. A.; White, J. G. *Z. Kristallogr.* **1978**, *147*, 177−186.
(3) Hiura, H.; Takahashi, H. *J. Phys. Chem.* **1992**, *96*, 8909−8915.
(4) Chernia, Z.; Livneh, T.; Pri-Bar, I.; Koresch, J. E. *Vib. Spectrosc.* **2001**, *25*, 119−131.
(5) Shimojima, A.; Takahashi, H. *J. Phys. Chem.* **1993**, *97*, 9103−9112.
(6) Tanizaki, Y.; Inoue, H.; Hoshi, T.; Shiraishi, J. *Z. Phys. Chem.* **1971**, *74*, 45−58.
(7) Okuyama, K.; Hasegawa, T.; Ito, M.; Mikami, N. *J. Phys. Chem.* **1984**, *88*, 1711−1716.
(8) Gutmann, M.; Gudipati, M.; Schönzart, P.-F.; Hohlneicher, G. *J. Phys. Chem.* **1992**, *96*, 2433−2442.
(9) Borst, R.; Chou, S. G.; Pratt, D. W. *Chem. Phys. Lett.* **2001**, *343*, 289−295.
(10) Hirata, Y.; Okada, T.; Mataga, N. *J. Phys. Chem.* **1992**, *96*, 6559−6563.
(11) Hirata, Y. *Bull. Chem. Soc. Jpn.* **1999**, *72*, 1647−1664.
(12) Ferrante, C.; Kensy, U.; Dick, B. *J. Phys. Chem.* **1993**, *97*, 13457−13463.
(13) Ishibashi, T.; Hamaguchi, H. *Chem. Phys. Lett.* **1997**, *264*, 551−555.
(14) Ishibashi, T.; Hamaguchi, H. *J. Phys. Chem. A* **1998**, *102*, 2263−2269.
(15) Ishibashi, T.; Okamoto, H.; Hamaguchi, H. *Chem. Phys. Lett.* **2000**, *325*, 212−218.
(16) Hamaguchi, H. *Acta Phys. Pol., A* **1999**, *95*, 37−48.
(17) Amatatsu, Y. *Chem. Phys. Lett.* **1999**, *314*, 364−368.
(18) Amatatsu, Y. *Chem. Phys.* **2001**, *274*, 87−98.
(19) Amatatsu, Y. *J. Comput. Chem.* **2002**, *23*, 928−937.
(20) Amatatsu, Y. *J. Comput. Chem.* **2002**, *23*, 950−956.
(21) Amatatsu, Y. *THEOCHEM* **2003**, *624*, 159−167.
(22) Schmidt, M. W.; Baldridge, K. K.; Boatz, J. A.; Elbert, S. T.; Gordon, M. S.; Jensen, J. H.; Koseki, S.; Matsunaga, N.; Nguyen, K. A.; Su, S. J.; Windus, T. L.; Dupuis, M.; Montgomery, J. A., Jr. *J. Comput. Chem.* **1993**, *14*, 1347−1363.
(23) Frisch, M. J.; Trucks, G. W.; Schlegel, H. B.; Scuseria, G. E.; Robb, M. A.; Cheeseman, J. R.; Montgomery, J. A., Jr.; Vreven, T.; Kudin, K. N.; Burant, J. C.; Millam, J. M.; Iyengar, S. S.; Tomasi, J.; Barone, V.; Mennucci, B.; Cossi, M.; Scalmani, G.; Rega, N.; Petersson, G. A.; Nakatsuji, H.; Hada, M.; Ehara, M.; Toyota, K.; Fukuda, R.; Hasegawa, J.; Ishida, M.; Nakajima, T.; Honda, Y.; Kitao, O.; Nakai, H.; Klene, M.; Li, X.; Knox, J. E.; Hratchian, H. P.; Cross, J. B.; Adamo, C.; Jaramillo, J.; Gomperts, R.; Stratmann, R. E.; Yazyev, O.; Austin, A. J.; Cammi, R.; Pomelli, C.; Ochterski, J. W.; Ayala, P. Y.; Morokuma, K.; Voth, G. A.; Salvador, P.; Dannenberg, J. J.; Zakrzewski, V. G.; Dapprich, S.; Daniels, A. D.; Strain, M. C.; Farkas, O.; Malick, D. K.; Rabuck, A. D.; Raghavachari, K.; Foresman, J. B.; Ortiz, J. V.; Cui, Q.; Baboul, A. G.; Clifford, S.; Cioslowski, J.; Stefanov, B. B.; Liu, G.; Liashenko, A.; Piskorz, P.; Komaromi, I.; Martin, R. L.; Fox, D. J.; Keith, T.; Al-Laham, M. A.; Peng, C. Y.; Nanayakkara, A.; Challacombe, M.; Gill, P. M. W.; Johnson, B.; Chen, W.; Wong, M. W.; Gonzalez, C.; Pople, J. A. *Gaussian 03*, revision B.04; Gaussian, Inc.: Pittsburgh, PA, 2003.